Surface Characterization of Nanoscale Co-Crystals Enabled through Tip Enhanced Raman Spectroscopy

Jakob Hübner,[*, a, b] Tanja Deckert-Gaudig,[c,d] Julien Glorian,[b] Volker Deckert [c, d, e] and Denis Spitzer [a, b]

[a] Nanomatériaux pour les Systèmes Sous Sollicitations Extrêmes (NS3E), ISL-CNRS-UNISTRA UMR 3208, French-German Research Institute of Saint-Louis, 5, rue du Général Cassagnou, B.P. 70034, 68301 Saint-Louis, France

[b] French-German Research Institute of Saint-Louis, 5, rue du Général Cassagnou, B.P. 70034, 68301 Saint-Louis, France

[c] Leibniz Institute of Photonic Technology (IPHT), Albert-Einsteinstr. 9, 07745 Jena, Germany

[d] Institute of Physical Chemistry and Abbe Center of Photonics, Friedrich-Schiller-University Jena, Helmholtzweg 4, 07743 Jena, Germany

[e] Institute of Quantum Science and Engineering, Texas A&M University, College Station, TX 77843-4242, USA

Supporting Information

Content

S1. AFM topographic mappings of n-CL-20/HMX nano-plates

In the following further AFM topographic maps of n-CL-20/HMX nano-plates recorded in non-contact mode are presented. n-CL-20/HMX nano-plates occur as single particles as well as agglomerates along their crystallographic bc-axis. Figure 1 shows one of these agglomerates. The substructure of single nano-plates can be identified easily from the AFM topographic image. n-CL-20/HMX agglomerates can be randomly orientated towards the scattering system. Therefore, only single CL-20/HMX nano-plates were investigated via AFM-TERS in this study. Figure 2 depict a selection of different single and agglomerated CL-20/HMX nano-plates to demonstrate that these structures appear in the whole sample.

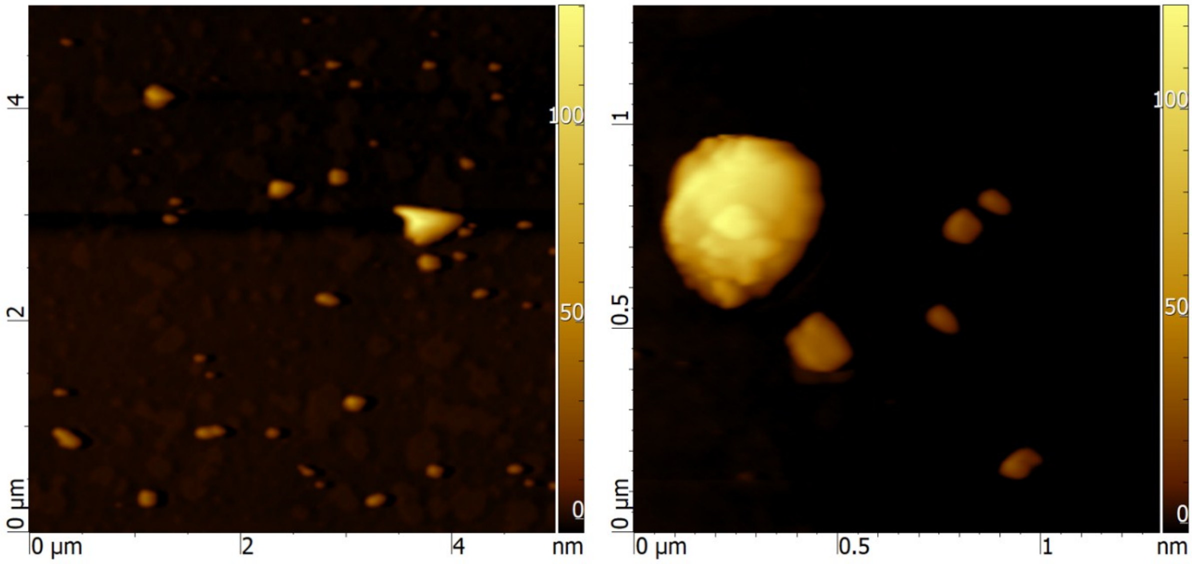

Figure 1. Left: AFM topographic mappings of several n-CL-20/HMX nano-plates. Single nano-plates show a height of ~30 nm. n-CL-20/HMX nano-plates built up agglomerates along their crystallographic bc-planes. **Right:** Single n-CL-20/HMX nano-plates and a CL-20/HMX nano-plate agglomerate.

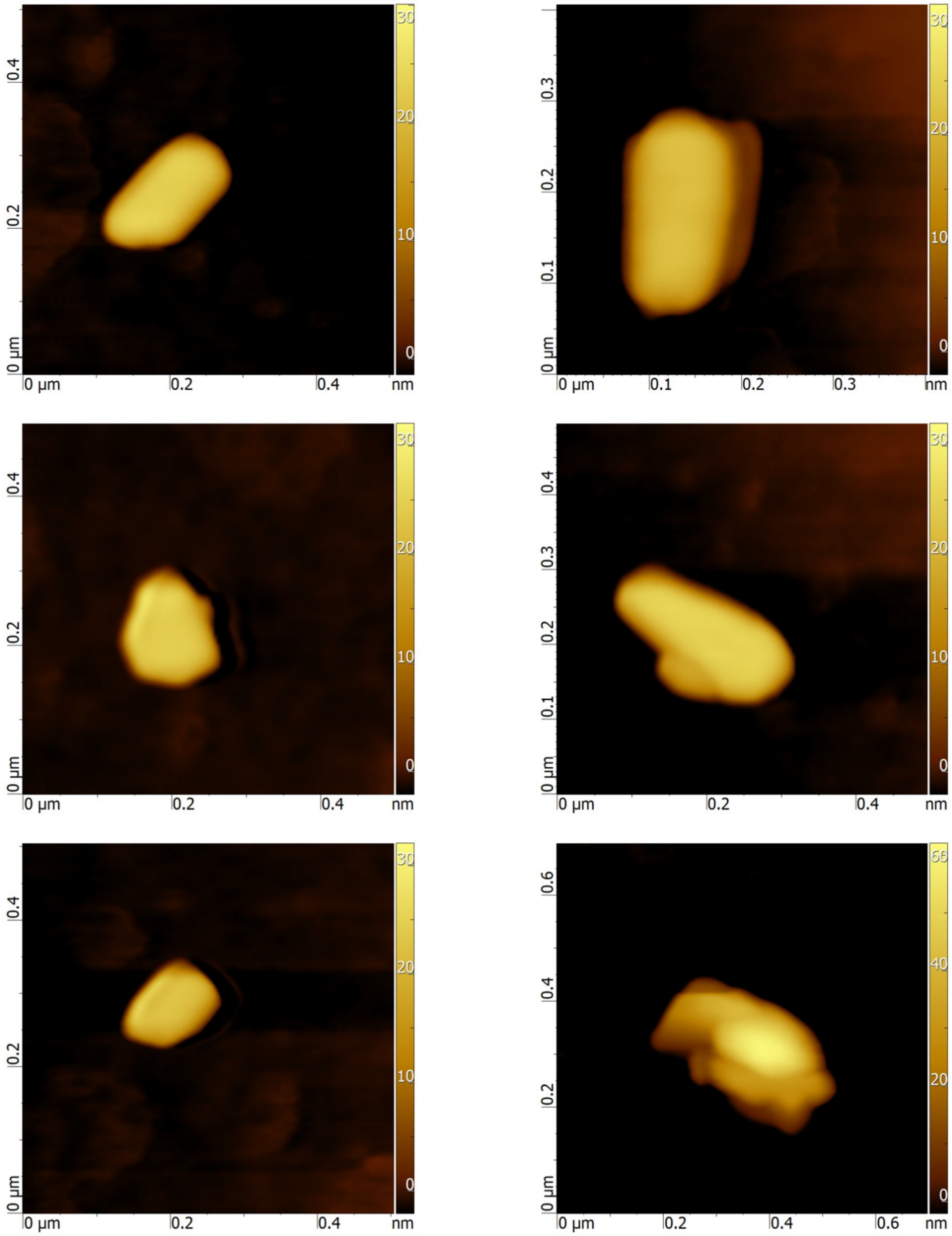

Figure 2. Selection of single and agglomerated n-CL-20/HMX nano-plates.

S2. Raman active vibrational frequencies and assignments

In the following Raman spectra and tables of Raman active vibrational frequencies of β-CL-20, γ-CL-20, β-HMX, CL-20/HMX as well as their assignments are presented.

β-CL-20

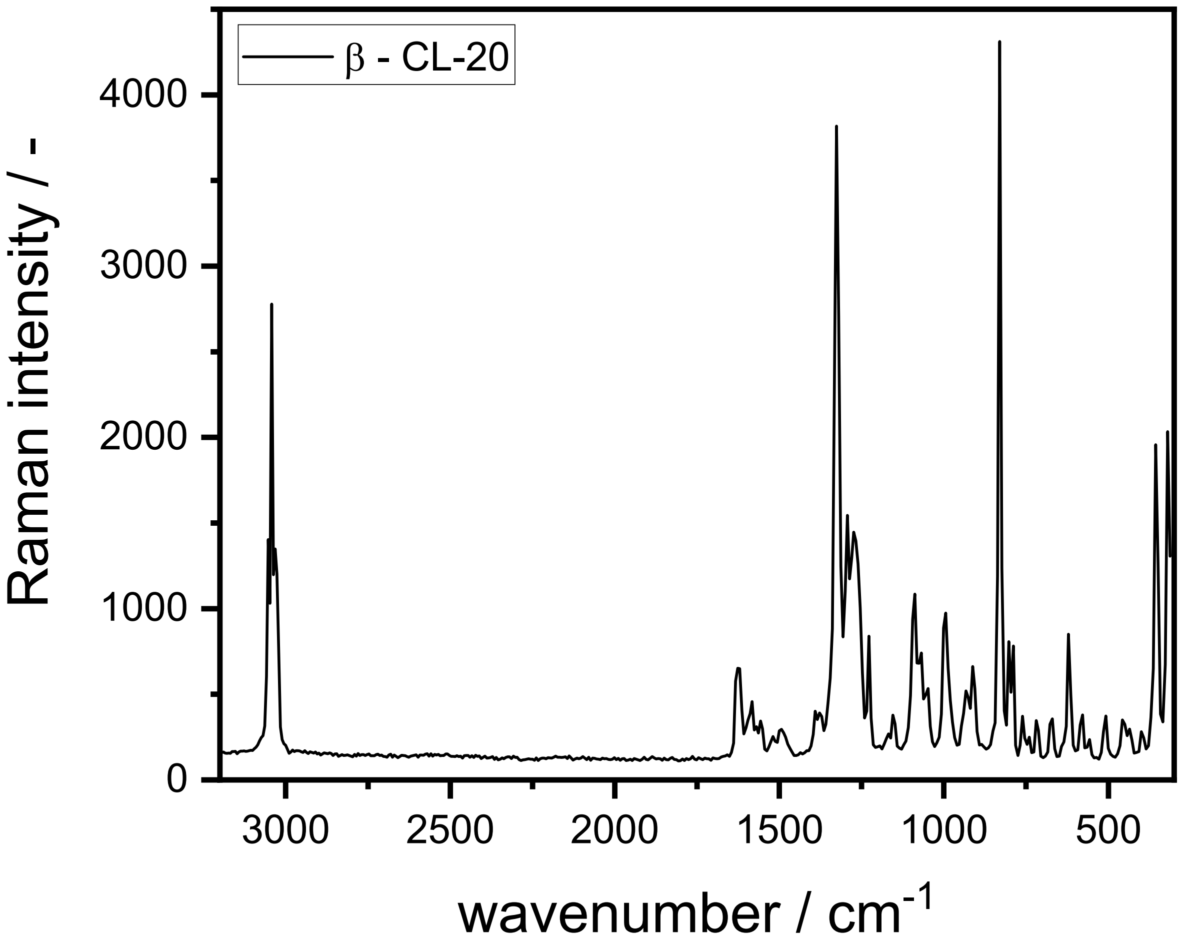

Figure 3. Raman spectrum of β-CL-20 in a spectral range between 3200 cm^{-1} and 300 cm^{-1}.

Table 1. Raman frequencies and their assignments of β-CL-20.

Raman frequencies of β-CL-20		
Experiment / cm^{-1}	**Literature / cm^{-1} [1]**	**Assignments [1]**
320 m	319 m	cage def, CNN bend
356 m	353, 369 w	cage def, N-NO_2 bend
400 vw	398 vw	N-NO_2 bend
436 vw	435 vw	N-NO_2 bend
457 vw	456 vw	N-NO_2 bend
507 vw	511 vw	NNO bend
557 vw	560 vw	cage def

579 vw	583 vw	cage def
621 w	621 w	cage def
670 vw	673 vw	NO bend
719 vw	718 vw	NO bend, NNO_2 bend
740 vw	744 vw	ONO bend
761 vw	762 vw	ONO bend
789 w	791w	ONO bend
803 w	803 w	ONO bend
830 vs	832 s	ring CH wag
913 w	912 w	ring str, ring CH wag
933 vw	932, 944 w	ring str, ring CH wag
994 w	982, 999 w	NN str
1048 vw	1052 vw	NN str
1068 w	1071 vw	NN str
1088 m	1093 w	NN str
1155 vw	1154 vw	CH bend
1228 w	1229 w	CH bend, NO str sym
1274 m	1276 m	CH bend, NO str sym
1293 m	1295 w	CH bend, NO str sym
1326 vs	1328 s	CH bend
1378 vw	1377 vw	CH bend
1391 vw	1390 vw	CH bend
1494 vw	1496 vw	CH bend
1557 vw	1557 vw	ONO str asym
1570 vw	1570 vw	ONO str asym
1582 w	1585 w	ONO str asym
1595 w	1593 w	ONO str asym
1626 m	1631 w	ONO str asym
3027 m	3027 w	CH str
3032 m	3036 m	CH str
3043 s	3045 s	CH str
3053 m	3056 m	CH str

β-CL 20 marker vibration (1595 cm^{-1}; ONO asymmetric stretching)) is marked in red. **Notes:** vs – very strong, s – strong, m – medium, w – weak, vw – very weak; asym – asymmetric, sym – symmetric, bend – bending, def – deformation, str – stretching, wag – wagging

γ-CL-20

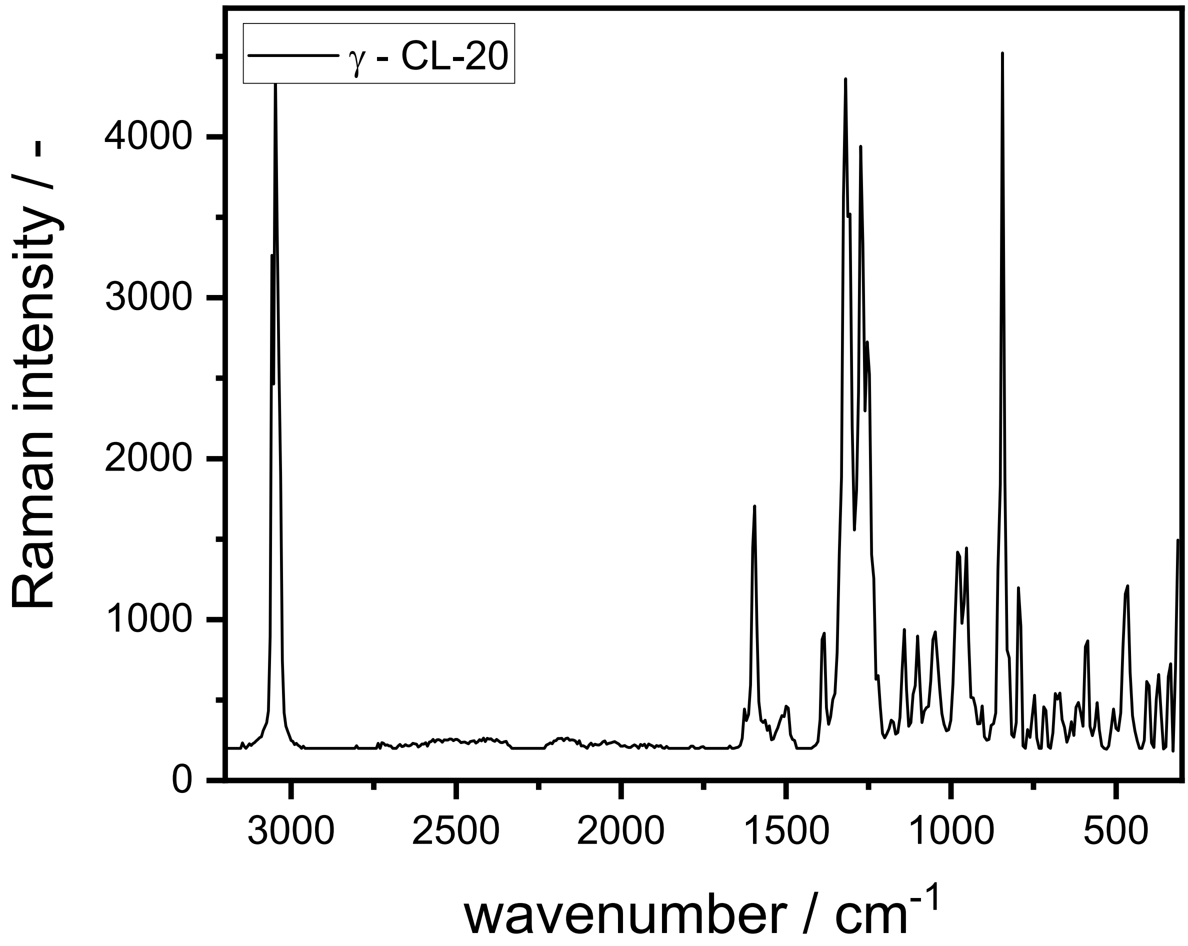

Figure 4. Raman spectrum of γ-CL-20 in a spectral range between 3200 cm^{-1} and 300 cm^{-1}.

Table 2. Raman frequencies and their assignments of γ-CL-20.

Raman frequencies of γ-CL-20		
Experiment / cm^{-1}	**Literature / cm^{-1} [1]**	**Assignments [1]**
312 m	318 m	cage def
334 w	340 vw	cage def
370 w	366 w	cage def
406 w	406 w	N-NO_2 bend
464 m	470, 479 vw	N-NO_2 bend
508 vw	512 w	N-NO_2 bend
557 vw	560 vw	N-NO_2 bend
585 w	592 w	cage def
614 vw	613, 619 w	cage def
635 vw	639 vw	cage def
684 w	686 vw	ONO bend

719 vw	718 w	ONO bend
747 w	750 vw	ONO bend
768 vw	770 vw	ONO bend
795 m	795, 807 w	ONO bend
823 w	827 vw	ONO bend
844 vs	846 m	ring CH wag
858 m	858 m	ring CH wag
878 vw	877 w	ring CH wag
906 vw	909	ring CH wag
933 w	935 vw	ring str, ring CH wag
953 m	956 w	ring str, ring CH wag
981 m	978 w	ring str, ring CH wag
1048 w	1055 w	ring str, NN str
1102 w	1105 w	NN str
1142 w	1145 m	CH bend, ring str
1182 vw	1179 w	CH bend, ring str
1221 w	1220 vw	CH bend
1234 m	1238 w	CH bend
1254 s	1254 m	CH bend, NO str sym
1273 s	1273 m	CH bend, NO str sym
1306 s	1310	CH bend, NO str sym
1319 vs	1324 s	CH bend, NO str sym
1338 m	1336 w	CH bend, NO str sym
1384 w	1389 w	CH bend
1500 vw	1498 vw	ONO str asym
1551 vw	1554 vw	ONO str asym
1563 vw	-	ONO str asym
1598 m	1600 m	ONO str asym
1627 vw	-	ONO str asym
3032 m	3034 s	CH str
3048 vs	3043, 3050 s	CH str
3059 s	3061 m	CH str

γ-CL 20 marker vibration (1598 cm^{-1}; ONO asymmetric stretching)) is marked in red. **Notes:** vs – very strong, s – strong, m – medium, w – weak, vw – very weak; asym – asymmetric, sym – symmetric, bend – bending, def – deformation, str – stretching, wag – wagging

β-HMX

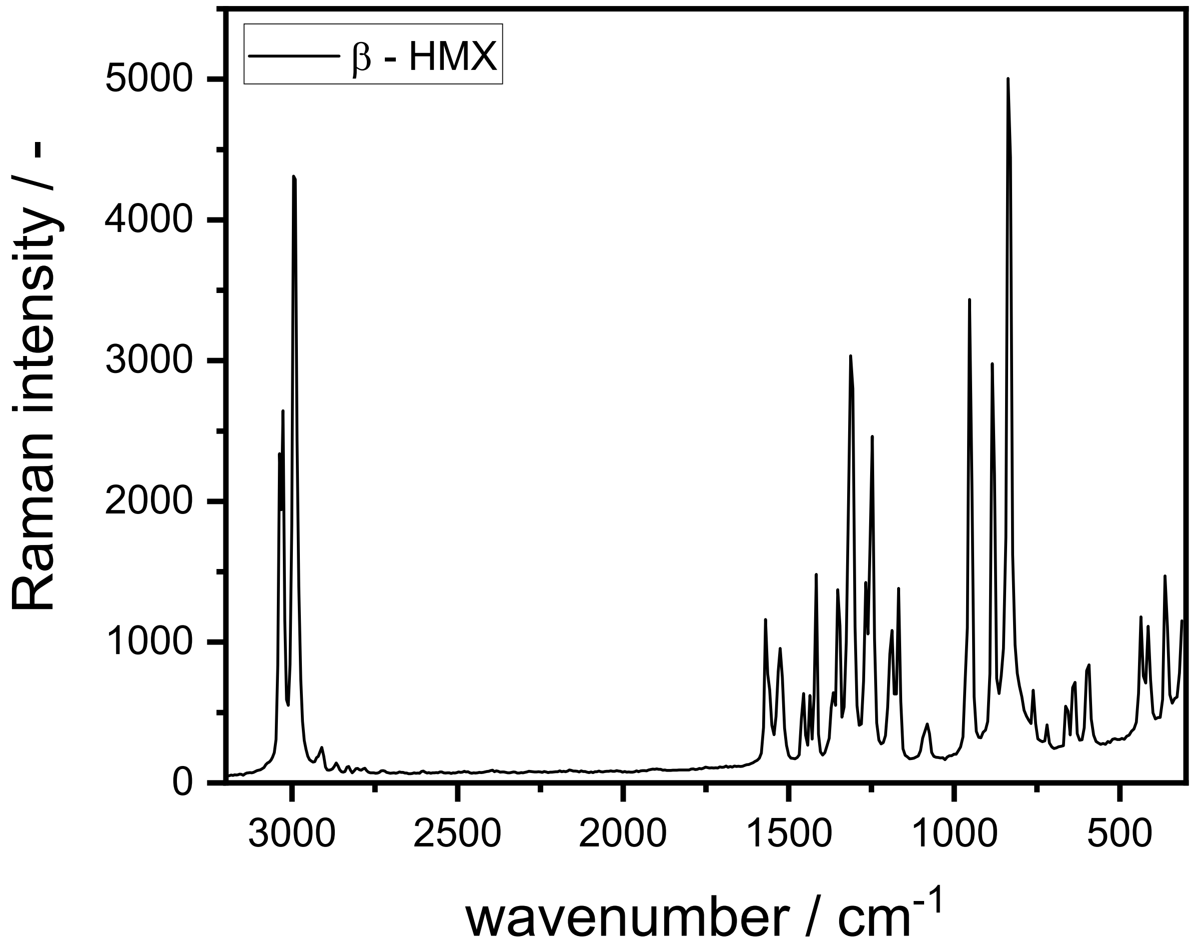

Figure 5. Raman spectrum of β-HMX in a spectral range between 3200 cm^{-1} and 300 cm^{-1}.

Table 3. Raman frequencies and their assignments of β-HMX.

Raman frequencies of β-HMX		
Experiment / cm^{-1}	**Literature / cm^{-1} [2-3]**	**Assignments [2]**
364 m	342	CN str, NN str, NCN bend
414 m	412	NNO bend, NNC bend
436 m	432	CNC bend, NNC bend
593 w	597	NNO bend
635 w	638	NNO bend, NN str
664 w	662	NNO bend, NN str
720 vw	721	ONO bend, CN str
761 v	759	ONO wag
837 vs	834	NC_2 str sym
885 s	881	NNC_2 str sym
954 s	950	NN str, CH_2 rock

967 w	965	CNN str asym, CH_2 rock
1082 vw	1090	NNC_2 str asym
1168 m	1168	CNN str asym, CH_2 rock
1188 m	1190	NC_2 str asym
1248 s	1248	NC_2 str asym
1267 m	1268	NO_2 str sym
1313 s	1312	CH_2 twist
1352 m	1350	CH_2 twist
1365 w	1368	CH_2 wag
1417 m	1418	CH_2 wag
1436 w	1438	HCH bend
1455 w	1460	HCH bend
1526 w	1532	NO_2 str asym
1570 m	1558	NO_2 str asym
2995 vs	2992	CH_2 str sym
3027 s	3028	CH_2 str asym
3038 s	3037	CH_2 str asym

β-HMX marker vibration (1417 cm^{-1}; CH_2 wagging) is marked in green. Notes: vs – very strong, s – strong, m – medium, w – weak, vw – very weak; asym – asymmetric, sym – symmetric, bend – bending, rock – rocking, str – stretching, twist – twisting, wag – wagging

CL-20/HMX (2:1) co-crystal

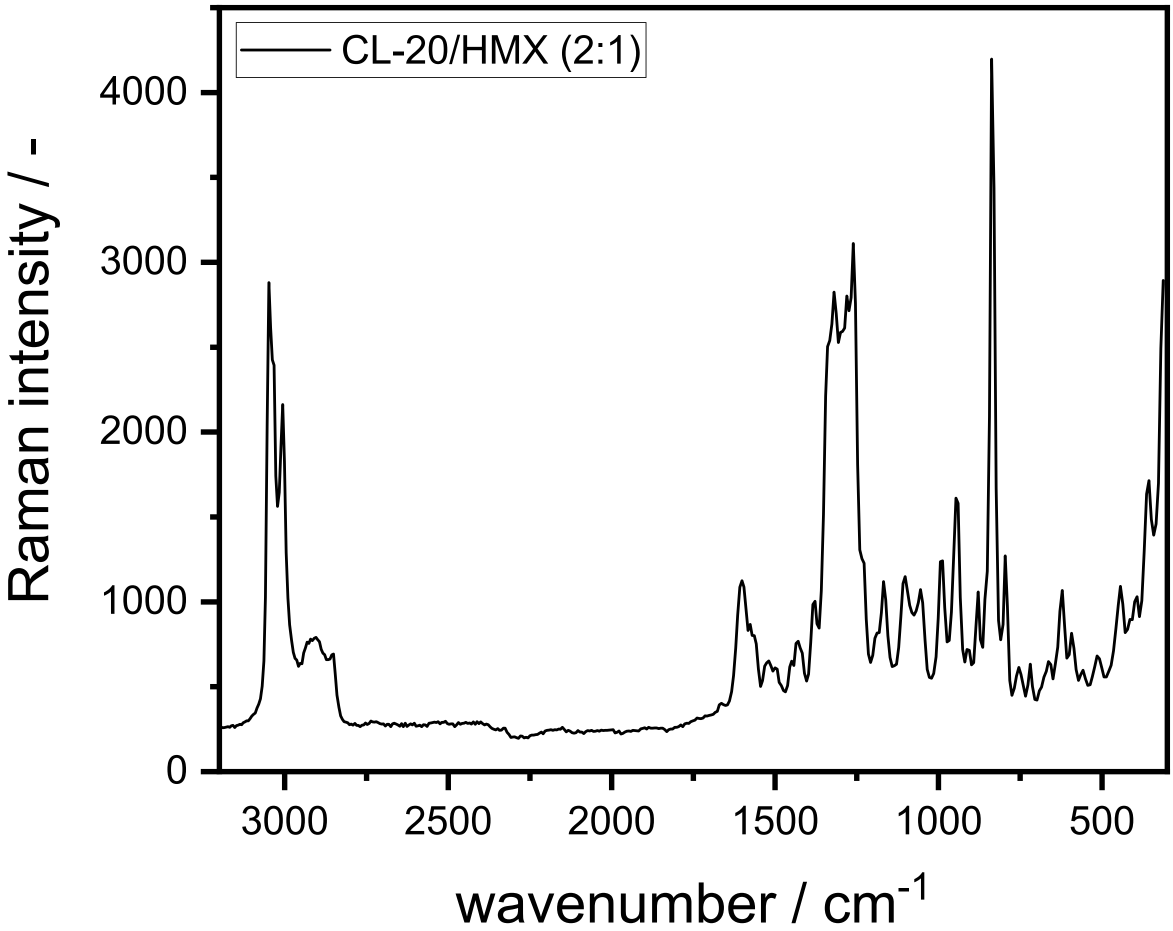

Figure 6. Raman spectrum of CL-20/HMX co-crystal (2:1) in a spectral range between 3200 cm^{-1} and 300 cm^{-1}.

Table 4. Raman frequencies and their assignments of CL-20/HMX.

Raman frequencies of CL-20/HMX (2:1)		
Experiment / cm^{-1}	**Literature / cm^{-1} (experimental) [4]**	**Assignments [4]**
356 m	360.4 w	**HMX**: ring def, CNC bend; **CL-20:** cage def
393 w	395.3 w	**CL-20:** CNC bend, N-NO_2 bend
414 w	415.1 w	**HMX:** NCN bend, N-NO_2 bend
443 w	441.1 m	**CL-20:** CNC bend, N-NO_2 bend
515 vw	515.9 w	**CL-20:** NCN bend, N-NO_2 bend, cage def
557 vw	560.5 w	**CL-20:** CNC bend, N-NO_2 bend
593 w	591.5 m	**CL-20:** cage def, CNC bend N-NO_2, bend

621 w	622.8 w	**CL-20:** cage def, N-NO_2 bend
656 w	658.2 w	**HMX:** cage def, ONO bend, CNC bend
664 w	665.7 vw	HMX: cage def, ONO bend, CNC bend
719 w	719.3 w	**CL-20:** cage def, N-NO_2 bend, CCN bend, **HMX:** ring def, CNC bend, ONO bend
754 w	755.8 w	**CL-20:** CCN bend, ONO bend
795 w	793.3 w	**HMX:** CNC bend, ONO bend
837 vs	835.4 vs	**CL-20:** ONO bend, NCN bend
858 w	856.0 m	**CL-20:** ONO bend, C-C str, N-N str
879 w	878.6 m	**HMX:** CNC str, N-N str, ONO bend
913 vw	908.3 w	**CL-20:** CNC str, CNC bend
947 m	942.1 m	**CL-20:** C-C str , N-N str
994 m	989.8 m	**CL-20:** C-C str, N-N str, ONO bend
1055 w	1053.7 m	**CL-20:** N-N str, ONO bend, CH wag
1102 m	1102.4 m	**CL-20:** NN tors, CH wag
1168 m	1167.2 m	**CL-20:** CNC str asym
1228 m	1230.3 m	**HMX:** CNC str asym
1260 s	1257.3 s	**CL-20:** CH wag; **HMX:** CNC str, ONO str
1280 s	1281.2 s	**CL-20:** CNC str asym, ONO str sym
1300 s	1301.7 s	**CL-20:** CH wag, ONO str sym
1320 s	1321.5 s	**CL-20:** CH bend, N-N str, ONO str sym
1340 s	1342.3 s	**CL-20:** CH wag, CN str, ONO str sym
1346 s	1353.1 w	CL-20: CH bend
1378 w	1372.8 w	**CL-20:** CH bend; **HMX:** CH_2 wag, ONO str sym, N-N str
1417 w	1413.9 w	**HMX:** CH_2 wag
1430 w	1432.4 m	**CL-20:** CH bend, CNC str
1500 vw	1505.8 w	**HMX:** CH_2 bend
1519 w	1517.2 w	**HMX:** CH_2 bend
1531 vw	1528.6 m	**HMX:** CH_2 bend
1563 w	1562.7 m	**HMX:** ONO str asym
1576 w	1575.8 m	**HMX:** ONO str asym
1595 m	1597.6 m	**CL-20:** ONO str asym
1602 m	1604.2 m	**CL-20:** ONO str asym
1608 m	1615.1 w	**CL-20:** ONO str asym
3006 s	3006.5 s	**HMX:** CH str
3016 s	3016.4 m	**HMX:** CH str
3032 s	3033.6 s	**CL-20:** CH str

3048 s	3050.8 vs	**CL-20:** CH str
3059 m	3059.3 m	**CL-20:** CH str

CL-20 marker vibration (1602cm^{-1}; ONO asymmetric stretching)) is marked in red, HMX marker vibration (1417 cm^{-1}, CH_2 wagging) is marked in green. **Notes:** vs – very strong, s – strong, m – medium, w – weak, vw – very weak; asym – asymmetric, sym – symmetric, bend – bending, rock – rocking, tors – torsion, str – stretching, twist – twisting, wag – wagging

S3. Calculation of approximated 3D normal coordinates

In a first step x-, y- and z-coordinates from all atoms which are involved mainly at the investigated molecular vibration were extracted from crystallographic data published by Bolton et al.[5] These atoms are depicted and numbered in Figure 7. As already described within the paper, the N atoms of the NO_2 functional groups of CL-20 oscillate oppositely to the O atoms. Furthermore, the atomic derivations from their equilibrium position are the same for all involved NO_2 groups. Thus, the vectors $\vec{q}_{m;\beta-CL-20}$, respectively $\vec{q}_{m;\gamma-CL-20}$, describe approximately the oscillation of the NO_2 group. These vectors are presented as yellow arrows in Figure 7. The directions of these vectors correspond to the direction of movement of the individual N atoms during the oscillation. These directions were determined by simulated molecular vibrations computed with Gaussian 16.

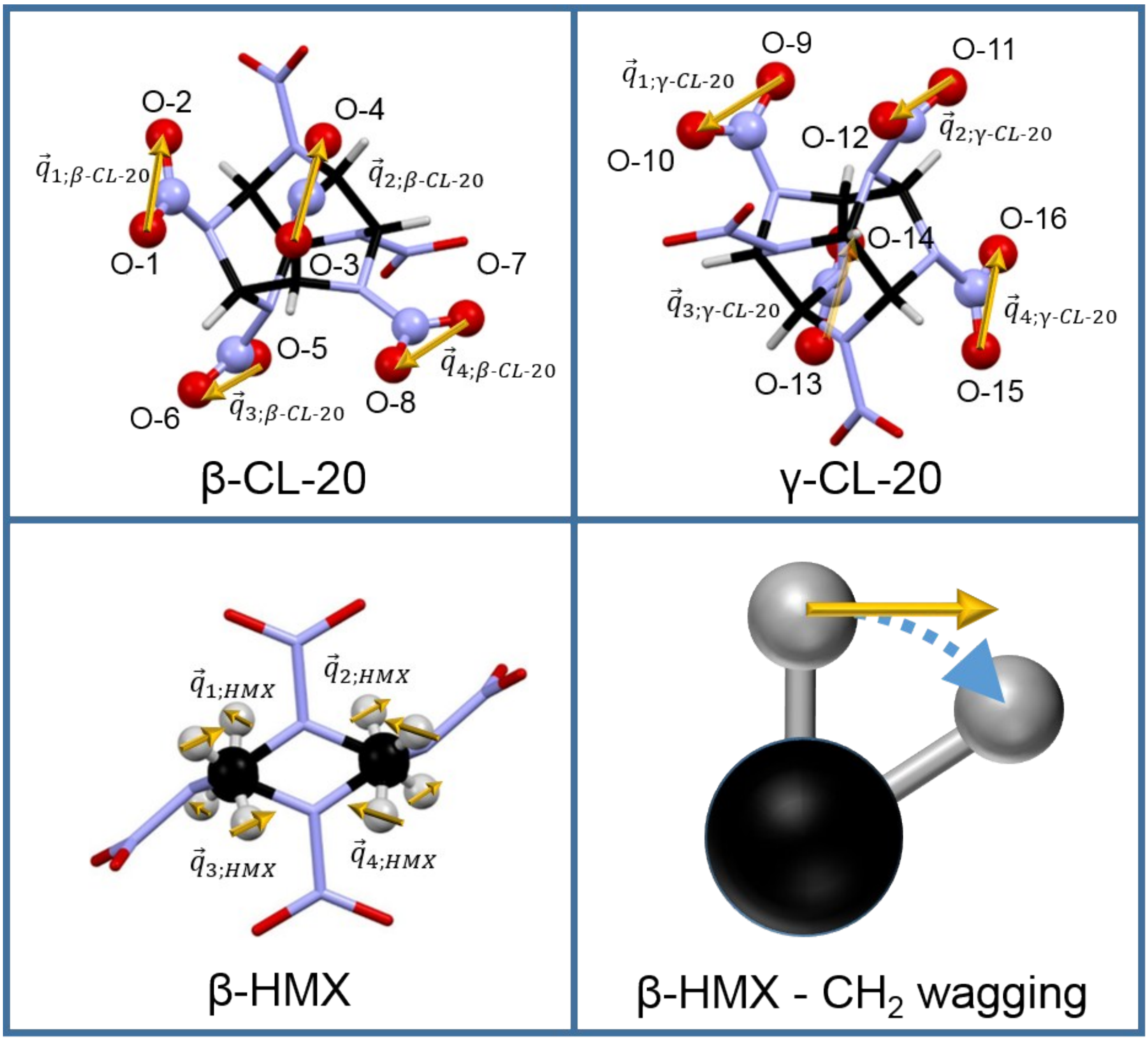

Figure 7. Atoms involved in the investigated normal modes. Yellow arrows represent vectors describing approximately oscillation directions of single functional groups.

The summation of $\vec{q}_{m;\beta-CL-20}$ and $\vec{q}_{m;\gamma-CL-20}$ leads to the approximated normal coordinates $\vec{q}_{0;\beta-CL-20}$ and $\vec{q}_{0;\gamma-CL-20}$ of the ONO asymmetric stretching vibrations of the CL-20 polymorphs. Since the Cartesian coordinates of crystallographic data do not correspond with that of the Raman scattering system, they had to be transformed. Calculations and number values of $\vec{q}_{0;\beta-CL-20}$ and $\vec{q}_{0;\gamma-CL-20}$ are summed up in Table 5 respectively Table 6.

Table 5. Calculation and number values of $\vec{q}_{0;\beta-CL-20}$

β-CL-20					
O-1		**O-2**		$\vec{q}_{1;\beta-CL-20}$	
x	12.245	**x**	14.052	**x**	1.807
y	6.907	**y**	5.850	**y**	-1.057
z	-4.246	**z**	-3.616	**z**	0.630
O-3		**O-4**		$\vec{q}_{2;\beta-CL-20}$	
x	11.561	**x**	13.450	**x**	1.889
y	9.040	**y**	8.479	**y**	-0.561
z	-1.344	**z**	-0.427	**z**	0.917
O-5		**O-6**		$\vec{q}_{3;\beta-CL-20}$	
x	9.328	**x**	8.866	**x**	-0.462
y	2.188	**y**	3.918	**y**	1.730
z	-2.549	**z**	-3.797	**z**	-1.248
O-7		**O-8**		$\vec{q}_{4;\beta-CL-20}$	
x	9.420	**x**	8.725	**x**	-0.695
y	5.985	**y**	7.270	**y**	1.285
z	1.867	**z**	0.255	**z**	-1.612
$\vec{q}_{0;\beta-CL-20}$		**crystal axis**	**projection**	$\vec{q}_{0;\beta-CL-20}$ **(in Raman scattering system)**	
x	2.539	**a**	**z → x**	**x**	1.397
y	1.397	**b**	**x → y**	**y**	-1.313
z	-1.313	**c**	**y → z**	**z**	2.539

Table 6. Calculation and number values of $\vec{q}_{0;\gamma-CL-20}$

γ-CL-20					
O-9		**O-10**		$\vec{q}_{1;\gamma-CL-20}$	
x	8.129	**x**	7.427	**x**	-0.702
y	3.647	**y**	4.858	**y**	1.211
z	0.511	**z**	-1.172	**z**	-1.683
O-11		**O-12**		$\vec{q}_{2;\gamma-CL-20}$	
x	7.479	**x**	7.018	**x**	-0.461
y	6.018	**y**	7.748	**y**	1.730
z	3.797	**z**	2.549	**z**	-1.248
O-13		**O-14**		$\vec{q}_{3;\gamma-CL-20}$	
x	2.896	**x**	4.785	**x**	1.889
y	1.457	**y**	0.896	**y**	-0.561
z	0.427	**z**	1.344	**z**	0.917
O-15		**O-16**		$\vec{q}_{4;\gamma-CL-20}$	
x	2.293	**x**	4.100	**x**	1.807
y	4.086	**y**	3.029	**y**	-1.057
z	3.616	**z**	4.246	**z**	0.630

$\vec{q}_{0;\gamma-CL-20}$		**crystal axis**	**projection**	$\vec{q}_{0;\gamma-CL-20}$ **(in Raman scattering system)**	
x	2.533	**a**	**z → x**	x	1.323
y	1.323	**b**	**x → y**	y	-1.384
z	-1.384	**c**	**y → z**	z	2.533

In case of the HMX CH_2 wagging vibration the path which is covered by the H is a circular segment around the central C atom. This movement can be described mathematically by a partially rotation of a plane defined by C and H atoms of a CH_2 functional group around the C atom. Thus the direction of this movement can be expressed approximately by the normal vector $\vec{q}_{m;HMX}$ of this plane at the equilibrium position (Figure 7, bottom right). The direction of these vectors and thus their algebraic signs are depicted in Figure 7 (bottom left). Here again the summation of $\vec{q}_{m;HMX}$ gives the approximated normal coordinate $\vec{q}_{0;HMX}$ of the HMX CH_2 wagging vibration. Since HMX molecules in β conformation appear as image and mirror image inside the CL-20/HMX co-crystal $\vec{q}_{0;HMX}$ has to be split into $\vec{q}_{0;HMX-1}$ and $\vec{q}_{0;HMX-2}$. The calculation and the number values of $\vec{q}_{0;HMX-1}$ and $\vec{q}_{0;HMX-2}$ can be found in Table 7 and Table 8. The approximated normal coordinate of both HMX conformations can be expressed as the average of $\vec{q}_{0;HMX-1}$ and $\vec{q}_{0;HMX-1}$:

Table 7. Calculation and number values of $\vec{q}_{0;HMX-1}$

β-HMX-1 (along b-axis)			
$\vec{q}_{1;HMX-1}$		$\vec{q}_{2;HMX-1}$	
x	-0.293	**x**	0.324
y	-0.531	**y**	0.444
z	0.795	**z**	0.835
$\vec{q}_{3;HMX-1}$		$\vec{q}_{4;HMX-1}$	
x	0.324	**x**	-0.293
y	0.444	**y**	-0.531
z	0.835	**z**	0.795
$\vec{q}_{0;HMX-1}$		**crystal axis**	**projection**
x	1.234	**a**	**z → x**
y	1.950	**b**	**x → y**
z	0.080	**c**	**y → z**
$\vec{q}_{0;HMX-1}$ **(in Raman scattering system)**			
x	0,080		
y	1,234		
z	1,950		

Table 8. Calculation and number values of $\vec{q}_{0;HMX-1}$

β-HMX-2 (along b-axis)			
$\vec{q}_{1;HMX-2}$		$\vec{q}_{2;HMX-2}$	
x	0.293	**x**	-0.324
y	0.531	**y**	-0.444
z	-0.795	**z**	-0.835
$\vec{q}_{3;HMX-2}$		$\vec{q}_{4;HMX-2}$	
x	-0.324	**x**	0.293

y	-0.444	y	0.531
z	-0.835	z	-0.795
$\vec{q}_{0;HMX-2}$		**crystal axis**	**projection**
x	1.234	a	z → x
y	1.950	b	x → y
z	0.080	c	y → z
$\vec{q}_{0;HMX-2}$ (in Raman scattering system)			
x	1.950		
y	0.080		
z	1.234		

The approximated normal coordinate of both HMX conformations can be expressed as the average of $\vec{q}_{0;HMX-1}$ and $\vec{q}_{0;HMX-1}$:

$$\vec{q}_{0;\beta HMX} = \frac{1}{2}\left(\frac{\sum_{m=1}^{4}\vec{q}_{m;\beta HMX-1}}{n_{\beta-HMX-1}} + \frac{\sum_{m=1}^{4}\vec{q}_{m;\beta HMX-2}}{n_{\beta-HMX-2}}\right) = \begin{pmatrix}1.950\\0.080\\1.234\end{pmatrix} \quad \text{Eq. 1}$$

In order to ensure a comparability of the approximated normal modes, $\vec{q}_{0;\beta CL20}$, $\vec{q}_{0;\gamma CL20}$ and $\vec{q}_{0;\beta HMX}$ are finally standardized. The standardization of the approximated normal mode vectors are depicted in Table 9.

Table 9. Standardization of approximated normal mode vectors

Standardization of $\vec{q}_{0;\beta HMX}$				
$\vec{q}_{0;\beta CL-20}$			**standardized $\vec{q}_{0;\beta CL-20}$**	
x	1.397	**factor:**	**x**	0.44
y	-1.313	3.182	**y**	-0.41
z	2.539		**z**	0.80
Standardization of $\vec{q}_{0;\beta HMX}$				
$\vec{q}_{0;\gamma CL20}$			**standardized $\vec{q}_{0;\gamma CL20}$**	
x	1.323	**factor:**	**x**	0.42
y	-1.384	3.175	**y**	-0.44
z	2.533		**z**	0.80
Standardization of $\vec{q}_{0;\beta HMX}$				

$\vec{q}_{0;\beta-HMX}$			**standardized** $\vec{q}_{0;\beta-HMX}$	
x	1.950	**factor:**	**x**	0.84
y	0.080	2.309	**y**	0.03
z	1.234		**z**	0.53

References

1. Ghosh, M.; Venkatesan, V.; Sikder, N.; Sikder, A. K., Quantitative Analysis of A-Cl-20 Polymorphic Impurity in E-Cl-20 Using Dispersive Raman Spectroscopy. *Central European Journal of Energetic Materials* **2013**, *10*.

2. Goetz, F.; Brill, T., Laser Raman Spectra of Alpha.-, Beta.-, Gamma.-, and Delta-Octahydro-1, 3, 5, 7-Tetranitro-1, 3, 5, 7-Tetrazocine and Their Temperature Dependence. *Journal of Physical Chemistry* **1979**, *83*, 340-346.

3. Brand, H. V.; Rabie, R. L.; Funk, D. J.; Diaz-Acosta, I.; Pulay, P.; Lippert, T. K., Theoretical and Experimental Study of the Vibrational Spectra of the A, B, and Δ Phases of Octahydro-1, 3, 5, 7-Tetranitro-1, 3, 5, 7-Tetrazocine (HMX). *The Journal of Physical Chemistry B* **2002**, *106*, 10594-10604.

4. Ghosh, M.; Sikder, A. K.; Banerjee, S.; Gonnade, R. G., Studies on Cl-20/Hmx (2: 1) Co-Crystal: A New Preparation Method, Structural and Thermo Kinetic Analysis. *Crystal Growth & Design* **2018**, *18*, 3781-3793.

5. Bolton, O.; Simke, L. R.; Pagoria, P. F.; Matzger, A. J., High Power Explosive with Good Sensitivity: A 2:1 Cocrystal of Cl-20:Hmx. *Crystal Growth & Design* **2012**, *12*, 4311-4314.